ORIGINAL PAPER

Comparison of different neurite density metrics with brain asymmetry evaluation

Ivan I. Maximov [a,b,c,*], **Lars T. Westlye** [a,b,d]

[a] Department of Psychology, University of Oslo, Oslo, Norway
[b] Norwegian Centre for Mental Disorders Research (NORMENT), Department of Mental Health and Addiction, Oslo University Hospital, Oslo, Norway
[c] Department of Health and Functioning, Western Norway University of Applied Sciences, Bergen, Norway
[d] KG Jensen Centre for Neurodevelopmental Disorders, University of Oslo, Oslo, Norway

Received 23 March 2023; accepted 13 July 2023

Abstract

The standard diffusion MRI model with intra- and extra-axonal water pools offers a set of microstructural parameters describing brain white matter architecture. However, non-linearities in the standard model and diffusion data contamination by noise and imaging artefacts make estimation of diffusion metrics challenging. In order to develop reliable diffusion approaches and to avoid computational model degeneracy, additional theoretical assumptions allowing stable numerical implementations are required. Advanced diffusion approaches allow for estimation of intra-axonal water fraction (AWF), describing a key structural characteristic of brain tissue. AWF can be interpreted as an indirect measure or proxy of neurite density and has a potential as useful clinical biomarker. Established diffusion approaches such as white matter tract integrity, neurite orientation dispersion and density imaging (NODDI), and spherical mean technique provide estimates of AWF within their respective theoretical frameworks. In the present study, we estimated AWF metrics using different diffusion approaches and compared measures of brain asymmetry between the different metrics in a sub-sample of 182 subjects from the UK Biobank. Multivariate decomposition by mean of linked independent component analysis revealed that the various AWF proxies derived from the different diffusion approaches reflect partly non-overlapping variance of independent components, with distinct anatomical distributions and sensitivity to age. Further, voxel-wise analysis revealed age-related differences in AWF-based brain asymmetry, indicating less apparent left-right hemisphere difference with higher age. Finally, we demonstrated that NODDI metrics suffer from a quite strong dependence on used numerical algorithms and post-processing pipeline. The analysis based on AWF metrics strongly depends on the used diffusion approach and leads to poorly reproducible results.

Keywords: Diffusion MRI; UK Biobank; Axonal water fraction; Brain asymmetry

Introduction

Diffusion MRI is a powerful non-invasive imaging technique allowing one to visualise and probe brain tissue at the micrometer scale *in vivo*. An important question arising in the interpretation of experimental diffusion data is how to connect the diffusion signal decay with underlying intra-voxel geometry and the organisation of complex living tissue [58,57,29]. Different diffusion approaches have been developed and applied to address this challenge, for example

* Corresponding author: Ivan I. Maximov, Department of Health and Functioning, Western Norway University of Applied Sciences, Bergen, Norway.
E-mail: ivan.maximov@hvl.no (I. I. Maximov).

Z Med Phys **xxx** (2023) xxx–xxx
https://doi.org/10.1016/j.zemedi.2023.07.003
www.elsevier.com/locate/zemedi

to artificial systems [22,44,78,50] in order to relate theoretical approaches with the known ground truth systems, animal models as a rich source of preclinical research information [36,28,18,60] and in the human brain *in vivo* (see books [37,38] and references therein).

Diffusion tensor imaging (DTI) [8] is the most popular diffusion approach, providing a set of scalar metrics that can be related to tissue integrity, such as fractional anisotropy (FA) or mean diffusivity, and various estimates of white matter (WM) connectivity using diffusion tensor tractography. Many attempts to fit the diffusion signal decay by different empirical functions have been made [58,30], e.g. cumulant expansion [33] or stretched-exponent [10]. The parameters of these functions do not explain the tissue architecture but can provide a visible contrast, in particular, in pathology. In parallel, researchers have tried to model WM and, partially, grey matter architecture by proposing a simplified representation of typical tissue compounds such as infinite cylinders, sticks and balls, impermeable spheres etc. [30]. The models include but are not limited to composite hindered and restricted model of diffusion (CHARMED) [6], extended CHARMED model with introduced diameter distribution of restricted cylindrical axons (AxCalibre) [7], neurite orientation distribution and density imaging (NODDI) [88], white matter tract integrity (WMTI) [21], spherical mean techniques (SMT) [41,40], restriction spectrum imaging [87], and other [29,30,58]. The different models have been developed and validated using either diffusion phantoms [22,44] or *ex vivo* measurements [28,34,25,36] including comparison with electron microscopy data [49,87,65,90]. This has led to the formulation of a standard diffusion model based on decomposition of diffusion pools into intra- and extra-axonal water compartments [58,57,30]. The standard diffusion model is primarily common to the most of the aforementioned approaches as a simplified description of WM tissue. However, each approach attracts its specific assumptions and relationships between diffusion parameters. These assumptions could be denied by the further research findings. Consequently, it leads to the difference in a practical realisation of the standard model. In the context of the standard diffusion model, measures of the intra-axonal water fraction (AWF) presents a useful indirect marker of neurite density in the brain and could be used for clinical research and diagnostics across a range of conditions [47,48,20].

Thus, AWF based on diffusion MRI represents a unique feature of the microstructure and organisation of human WM. Measures of AWF might provide sensitive biomarkers for understanding brain aging [71,42], genome-wide association studies [19], and brain and mental disorders [56]. Although attributed similar biophysical properties, the AWF metrics provided by the different implementations of the standard model may diverge due to theoretical and model-specific assumptions. However, there is still a lack of direct group comparison between different approaches using realistic human MRI data [31,32,11].

The UK Biobank (UKB) diffusion protocol [54,2] is one of the most used diffusion schemes in research and clinical studies, and the use of multi-shell diffusion imaging and many encoding directions enables the implementation of a set of biophysical models including the abovementioned diffusion approaches. Hence, UKB is an excellent source for statistical validation of diffusion models, in particular, in cases with unknown ground truth. UKB offers a set of pre-estimated diffusion metrics, including DTI and NODDI, and raw data for additional analysis [54]. These microstructural diffusion-based properties of the human brain allow scholars to discover general brain patterns and imaging phenotypes that are sensitive to variability in physiological, genetic and demographic features [71]. As an interesting application of AWF measure, we use brain asymmetry [66,74,73,61]. The brain asymmetry index [76,5] represents a relevant metric for comparison of the AWF estimations due to a concealment of the obvious difference between the AWF metrics derived from the different diffusion approaches. As a result, it is feasible to expect some dependence of asymmetry index on age and likely other parameters in WM.

In this work we investigated the consistency between neurite density metrics derived from three popular diffusion approaches (WMTI, NODDI, and SMT). Due to the time-consuming computations of NODDI parameters, it is important to test the consistency and reliability of NODDI metrics derived from different post-processing pipelines [2,51] and numerical algorithms [88,12]. To evaluate the feasibility of the estimated neurite density indices as surrogate imaging biomarkers, we compared brain WM asymmetry measures between the different implementations and their associations with age. We used a combination of univariate voxel-wise analysis with permutation-based inference, data-driven multimodal decomposition using linked independent component analysis (LICA), and structural similarity analysis, which allowed for a comprehensive assessment of brain asymmetry patterns based on various AWF metrics.

Materials and Methods

Participants and MRI data

In the present study we used 182 participants (age: min = 40.24; max = 70.11; mean = 54.70; std = 9.35 years), (sex: male = 90; female = 92), (right-handed = 151, left-handed = 27, ambidexters = 4) randomly selected in order to uniformly cover the UKB age range between 40 and 70 years. An overview of the UKB data acquisition, protocol parameters, and image validation can be found in [2,54].

Please cite this article as: I.I. Maximov and L.T. Westlye, Comparison of different neurite density metrics with brain asymmetry evaluation, Z Med Phys, https://doi.org/10.1016/j.zemedi.2023.07.003

Briefly, a conventional Stejskal-Tanner monopolar spin-echo echo-planar imaging (EPI) sequence was used with multiband factor 3, diffusion weightings were $b = 1$ and 2 ms/μm^2 and 50 non-coplanar diffusion directions per diffusion shell. All selected subjects were scanned at a single 3T Siemens Skyra scanner with a standard Siemens 32-channel head coil, in Cheadle, Manchester, UK. The spatial resolution was 2 mm^3 isotropic, and 5 AP vs 3 PA images with $b = 0$ ms/μm^2 were acquired. All diffusion data were post-processed using an optimised diffusion pipeline [51] consisting of 7 steps: noise correction [80], Gibbs-ringing correction [43], estimation of echo-planar imaging distortions, motion, eddy-current and susceptibility distortion corrections including outlier detection and reestimation [4,3], field non-uniformity correction [77], spatial smoothing using *fslmaths* from FSL package [70] with the Gaussian kernel 1 mm^3, and diffusion metrics estimation. A data quality was estimated by temporal signal-to-noise ratio [64] for each *b*-shell. Original UKB data, supplied by UKB, were estimated using UKB pipeline [2] including susceptibility, eddy-current, and head motion corrections accompanied with slice outlier detection and replacement [3,4]. The original UKB scalar NODDI metrics were computed using Python implementation of the Accelerated Microstructure Imaging via Convex Optimisation (AMICO) algorithm [12] of NODDI model [88].

Diffusion approaches

In order to derive neurite density metrics based on intra-axonal water fraction we chose three commonly applied biophysical approaches derived from the standard diffusion model [58]: WMTI, NODDI, and SMT. These diffusion approaches are feasible for similar protocols with high diffusion weightings [9]. Below we briefly describe each approach.

WMTI

In terms of the standard diffusion model, WMTI assumes two water compartments: intra- and extra-axonal spaces. As a result, WMTI models the intra-axonal space as a parallel bundle of cylinders with effective radius equals to zero [21]. The cylinders are impermeable, i.e., there are no water exchange between intra- and extra-axonal spaces. The extra-axonal space is described by anisotropic but still Gaussian diffusion. In order to keep the model simple, a few more assumptions have been made: that the intra-axonal space consists of mostly myelinated axons without any contribution from myelin due to fast relaxation rate across of typical diffusion times; at the same time in extra-axonal space the glial cells possess fast water exchange with extra-cellular matrix; both intra- and extra-axonal spaces are modelled by Gaussian diffusion tensors [21,31]. In order to avoid degeneration, it is incorrectly assumed that intra-axonal diffusion is slower than diffusion in the extra-axonal matrix. Besides, WMTI parametrisation works in the case of a coherent or parallel axonal bundle. Some estimations allow to have an orientation dispersion up to 30°. WMTI output consists of axonal water fraction (*AWF*), extra-axonal diffusivities: axial and radial components. The scalar metrics were estimated using the original Matlab scripts (MathWorks, Natick, MA USA) from Veraart and colleagues [81]. It is worth considering that the WMTI approach is not valid in the case of crossing fibres or high orientation dispersion. Additionally, the assumption about the slower intra-axonal diffusivity did not find its confirmation in the recent publications [14,35]. Thus, WMTI should be interpreted with a caution.

NODDI

NODDI introduces three water compartments: intra- and extra-axonal spaces and isotropic water pool responsible for cerebrospinal fluid contamination [88]. The NODDI approach assumes that the axon orientation dispersion can be described by an axially symmetric function, such as Watson [88] or Bingham [75] functions. In turn, both intra- and extra-axonal diffusivities parallel to the bundle axis are fixed to a given value (in the case of adults to 1.7 μm^2/ms). The radial diffusivity in extra-axonal space is determined by the tortuosity model [72]: $D^{\text{extra}}{}_{\perp} = D^{\text{extra}}{}_{\parallel}\,(1 - f_{\text{ic}})$, where D^{extra} are the extra-axonal radial ($\perp$ and axial ($\parallel$) diffusion coefficients, respectively; f_{ic} is the intra-axonal water fraction. Water diffusion in isotropic compartment is fixed to 3 μm^2/ms. NODDI is computationally demanding. In order to accelerate the estimation of geometrical parameters, such as orientation dispersion and water fractions, Daducci and colleagues [12] decomposed and linearised the problem using information about a bundle orientation from a DTI metric. This significantly reduced computation time per subject. The NODDI approach output consists of intra-axonal water fraction (*icvf* for original NODDI metric, and *ICVF* for AMICO derived metric in our notation), isotropic water fraction, and orientation neurite dispersion. We estimated NODDI parameters using the Matlab scripts for original NODDI [88] and for AMICO acceleration [12]. In our work, the UKB pre-estimated intra-axonal water fraction shared by UKB is defined as *UICVF*. NODDI assumptions such as coincidence of intra- and extra-axonal axial diffusivities and its fixation did not find a confirmation in the recent publications [14,27].

SMT

Estimating orientation dispersion in the axon bundles is a complex theoretical problem [57], in particular, using standard diffusion sequence protocols [63,59]. Recent achieve-

Please cite this article as: I.I. Maximov and L.T. Westlye, Comparison of different neurite density metrics with brain asymmetry evaluation, Z Med Phys, https://doi.org/10.1016/j.zemedi.2023.07.003

ments in isotropic diffusion weightings [85,36,79] and double diffusion encoding [26,67] allowed one to avoid problems associated with standard model degeneration. Instead of requiring a new pulse sequence on the clinical scanners one can recall a similar approach using a powder averaging technique [41] for both one and two compartment models [40]. Nevertheless, the averaged signal still possesses a quite flat-fitting landscape, which might lead to degeneracy as in the case of NODDI [31,32,26]. Kaden et al. [40] increased the stability of the optimisation procedure by the following additional assumptions: diffusivity determines by the tortuosity model [72], axial diffusivity in intra- and extra-axonal spaces are equal, and axons are presented as sticks, i.e. radial inta-axonal diffusion is equal to zero. In the present work we consider two compartment spherical mean technique [40] allowing one to extract a neurite density metric. Note that SMT does not model free water contamination similar to WMTI approach, however, allows one to model the orientation dispersion. SMT output consists of intra-axonal water fraction (*intra*), intra-axonal diffusivity, and extra-axonal diffusivities: mean and radial components, and micro FA. We estimated SMT metrics using the original SMT code (https://github.com/ekaden/smt). Similar to the NODDI assumptions, the SMT approach demands an equality of intra- and extra-axonal axial diffusivities. This assumption was not approved by the recently published results [26,36].

Tract Based Spatial Statistics (TBSS)

In order to compare different diffusion metrics and approaches, we applied voxel-wise analysis using TBSS [69]. Initially, all volumes were aligned to the FMRI58_FA template, supplied by FSL [70], using a non-linear transformation implemented by FNIRT [70]. Next, a mean FA images of all subjects was obtained and thinned in order to create mean FA skeleton. Afterwards, the subject's FA values are projected onto the mean skeleton, by filling the skeleton with FA values from the nearest relevant tract centre. The skeleton-based analysis allows one to minimise confounding effects due to partial voluming and any residual misalignments originating from non-linear spatial transformations. Additionally, the TBSS derived skeleton is used for averaging of diffusion metrics over the skeleton.

We performed voxel-wise comparisons of NODDI scalar metrics obtained from two pipelines and different algorithm implementations using general linear models (GLM). For simplicity, we used individual level difference maps (M_A-M_B, where M is the scalar metric, and A/B are the algorithm or pipeline index) including age and sex as covariates. For all contrasts, statistical analysis was performed using permutation-based inference implemented in *randomise* with 5000 permutations. Threshold-free cluster enhancement (TFCE) was used [68]. Statistical p-value maps were thresholded at $p < 0.05$ corrected for multiple comparisons across space.

Brain asymmetry analysis was performed using the symmetrised TBSS skeleton produced by the FSL utility *tbss_sym*. The script generated the symmetric mean FA image and derived symmetric skeleton. Next, the difference maps between left-right hemispheres are tested voxel-wise for each diffusion metric using an appropriate design matrix and contrast files with age and sex as covariates by the *randomise* function with 5000 permutations. Statistical p-value maps were thresholded at $p < 0.05$ corrected for multiple comparisons as well. Analysis of averaged asymmetry index for different diffusion approaches was performed using a Kruskal-Wallis test and *kruskalwallis* MATLAB function. It included post hoc analysis with Bonferroni corrections for the multiple comparisons.

Linked independent component analysis (LICA)

In order to model inter-subject variability across the diffusion metrics we performed data-driven decomposition based on LICA from the FSL package [23,24]. LICA is based on the conventional ICA technique, assuming that the signal presents a linear mixture of statistically independent spatial patterns. LICA iteratively searches maximally non-Gaussian patterns by subject weight updating. The resulting LICA components are characterised by group spatial maps and corresponding individual subject weights. The model order was defined using cophenetic coefficient estimation [62]. LICA allows us to decompose independent multimodal spatial patterns across different imaging phenotypes [16,23,24]. We would expect that images assumed to reflect similar biological properties, such as axonal water fraction, would show large degree of fusing, reflecting their shared variance, i.e. one does not expect to find any dominating (unique) AWF metric.

The AWF metrics and FA maps were included in the LICA decomposition in order to evaluate the common and unique inter-subject variability across the six parameters taking into account differences in the pipeline and NODDI algorithm evaluations. Namely, FA from DKI, *AWF* from WMTI, *intra* from SMT, *icvf* from original NODDI and optimised pipeline, *ICVF* from AMICO NODDI and optimised pipeline, and *UICVF* from AMICO NODDI and UKB pipeline. Since FA are not assumed to reflect direct neurite density we repeated LICA without FA maps as well. All LICA runs were performed using TBSS skeletons with 1 mm^3 resolution and 3000 iterations.

Statistical analysis

Diffusion metrics and associated global asymmetry indices ($AI = [M_R - M_L]/[M_R + M_L]$, where R/L are the

Please cite this article as: I.I. Maximov and L.T. Westlye, Comparison of different neurite density metrics with brain asymmetry evaluation, Z Med Phys, https://doi.org/10.1016/j.zemedi.2023.07.003

right- or left-hemisphere values of metric *M*, respectively) were compared using general linear model (GLM) $AI = b_0 + b_1$ Age $+ b_2$ Sex. Global AI was computed by averaging the voxel-wise AI maps. The GLM fit was performed using Matlab function *lmfit*. The linear correlations between skeleton-averaged diffusion metrics and global AI values were estimated using Matlab function *corr,* which produced a Pearson correlation coefficient.

In order to provide a quantitative comparison between the skeleton maps we used structural similarity (SSIM) metric [83]. SSIM allows one to estimate three basic parameters of the image in accordance with the reference image: luminance, contrast, and structure, and has been used in MR image evaluations [53,82]. For SSIM we used Matlab function *ssim*. In order to present a qualitative estimation of SSIM values in the case of TBSS pipeline, we presented a distribution of SSIM values for intra metrics in Supplementary Material as well as simple simulations for skeleton based images and their influence on SSIM estimation.

Results

In order to estimate correlations between all diffusion metrics, we averaged each metric over the TBSS skeleton for each subject. Fig. 1 shows the scatter plots of mean skeleton FA and estimated axonal water fractions from WMTI, SMT, and NODDI models. FA demonstrated the lowest correlation coefficients among all diffusion metrics. The original NODDI metric (*icvf*) exhibits the same correlations (r = 0.97) with *ICVF* and *UICVF* values, in contrast to the lower correlation (r = 0.94) between the two NODDI AMICO metrics *ICVF* and *UICVF*. The *AWF* and *intra* (r = 0.97) metrics show a lower correlation (r = 0.92) with *ICVF* values. The histogram mode of axonal water fraction (0.39) for *AWF* values is lower than the modes ($\approx$ 0.59) of all other metrics.

Fig. 2 shows the results of LICA analysis using 20 independent components (IC) in two cases: with and without FA. Fig. 2 shows the contribution of different diffusion metrics to each IC. The weights coefficient correlations of all subjects for 20 IC in both cases with and without FA metric are presented as well. As an example of common variation patterns, we present IC number 1 and 15. In the case of IC1 we find contribution from all diffusion metrics with the strongest contribution from *icfv* (25%) and *ICVF* (25%) metrics and lowest contribution from FA. Notably, all diffusion metrics, including FA, contribute in spatial patterns distributed over the most part of TBSS skeleton. In contrast, IC15 reflects contributions from *UICVF* only (98%) with negligible interaction of ICVF metrics (1%). Mapped spatial pattern of IC15 is similar to the behaviour of IC17 with ICVF metric (96%) (not presented in Fig. 2). IC15 exhibits the remarkable spatial patterns of the common variance (see Fig. 2d).

In order to find spatial patterns with significant differences on the brain skeleton between the three NODDI approaches, we applied TBSS analysis for three NODDI-derived diffusion metrics (axon water fraction, isotropic water fraction, and neurite orientation dispersion). Fig. 3 demonstrates the results of the TBSS analysis between two pairs of approaches: *a*) comparison between original NODDI and NODDI AMICO using the same optimised pipeline; *b*) comparison between optimised and UKB pipelines for NODDI AMICO algorithm implemented in Matlab (optimised pipeline) and in Python (UKB pipeline). Briefly, the difference between original NODDI and AMICO NODDI using the optimised pipeline covers a large part of the brain skeleton and presents mainly a global offset shift. The shift appears in all NODDI-derived metrics. The comparison between the same NODDI AMICO metrics obtained using different pipelines revealed more complex patterns with under- and overestimated values. The differences are found in all NODDI metrics.

Fig. 4 shows the results from the TBSS asymmetry analysis. All diffusion metrics demonstrated regions with significant asymmetry. In order to perform a pairwise comparison between statistically significant spatial patterns on the skeleton, we computed structural similarities between all image pairs. The results are presented in Table 1. The structural similarities are estimated for two cases: the values from the left hemisphere are higher than in the right hemisphere, and in the opposite case, the values from the left hemisphere are lower than in the right hemisphere. These values are presented in the table cells over the main diagonal (the main diagonal marked by the red colour). The values below the main diagonal present a ratio between a number of common voxel and the total number of voxels with significant differences, i.e. $R = N_A \cap N_B / N_A$, where N_A is the number of voxels in estimated skeleton region, and N_B is the number of voxels in skeleton region for a pair comparison. The comparison reveals that the spatial patterns with significant difference localised by *UICVF* metric demonstrate lower structural similarities among other diffusion metrics and a lower proportion of common skeleton voxels with significant difference. In turn, *icvf* and *ICVF* metrics demonstrate high level of proximity in both the structural similarities and number of the common voxels. The mean overlap between *AWF*, *intra* and *icvf* maps for higher and lower metrics in left hemisphere were *AWF* = 0.7913/0.5745; *intra* = 0.8254/0.6359; *icvf* = 0.8358/0.6098, respectively, suggesting that the *intra* metric (SMT) had the highest overlapping rate among all AWF metrics.

Fig. 5 shows scatterplots of diffusion metrics and their respective AI values. The axon water fractions derived from NODDI showed weak positive correlations for AI vs *ICVF*

Please cite this article as: I.I. Maximov and L.T. Westlye, Comparison of different neurite density metrics with brain asymmetry evaluation, Z Med Phys, https://doi.org/10.1016/j.zemedi.2023.07.003

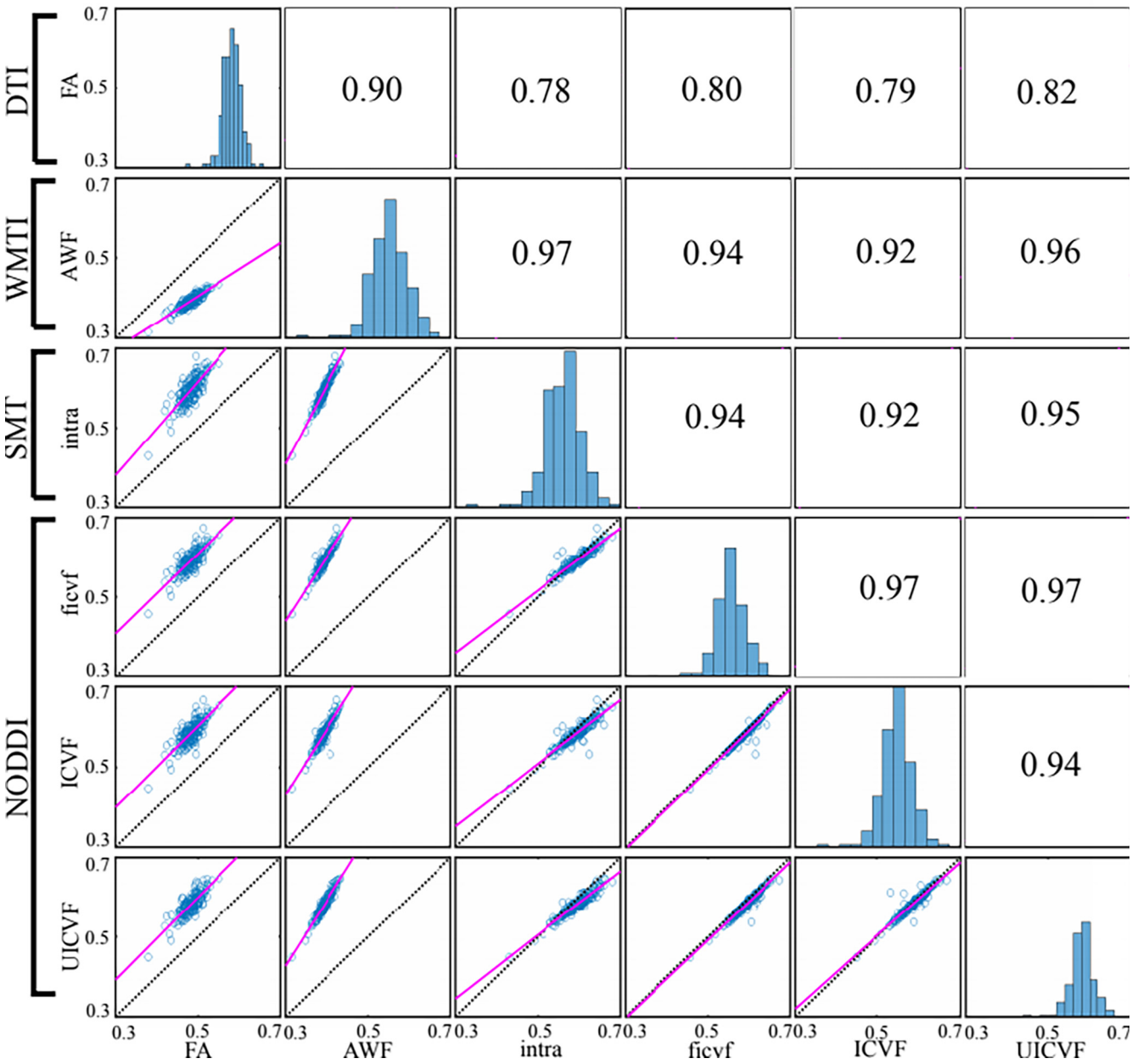

Figure 1. Correlation plots for FA and axonal water fractions obtained from WMTI (AWF), SMT (intra), and NODDI: original algorithm and optimised pipeline (ficvf); NODDI AMICO algorithm and optimised pipeline (ICVF); and NODDI AMICO algorithm and UKB pipeline (UICVF). All diffusion metrics were averaged over subject's skeletons in accordance with TBSS pipeline. Black dotted lines are a unity; margenta lines are a result of linear regression. Upper diagonal shows the corresponding correlation coefficients. Histograms on the main diagonal present a distribution of mean skeleton values for each diffusion metric.

and negative correlations for AI vs (*icvf*, *UICVF*). The correlations between AI and (FA, *AWF*, *intra*) were also weak. For FA, higher anisotropy was weakly associated with more negative AI, i.e. stronger right-left asymmetry. The association between AI and (*AWF*, *intra*) were positive, with higher axon water fraction with more positive AI.

In order to compare averaged AI derived from different diffusion approaches we visualised AI using boxplots in Fig. 6. The Kruskal-Wallis test demonstrated that all diffusion metrics are different including (one-side p-value < 1e-99) and excluding (one-side p-value < 0.003) FA values. Post hoc analysis allowed us to reveal that AI means for icvf

Please cite this article as: I.I. Maximov and L.T. Westlye, Comparison of different neurite density metrics with brain asymmetry evaluation, Z Med Phys, https://doi.org/10.1016/j.zemedi.2023.07.003

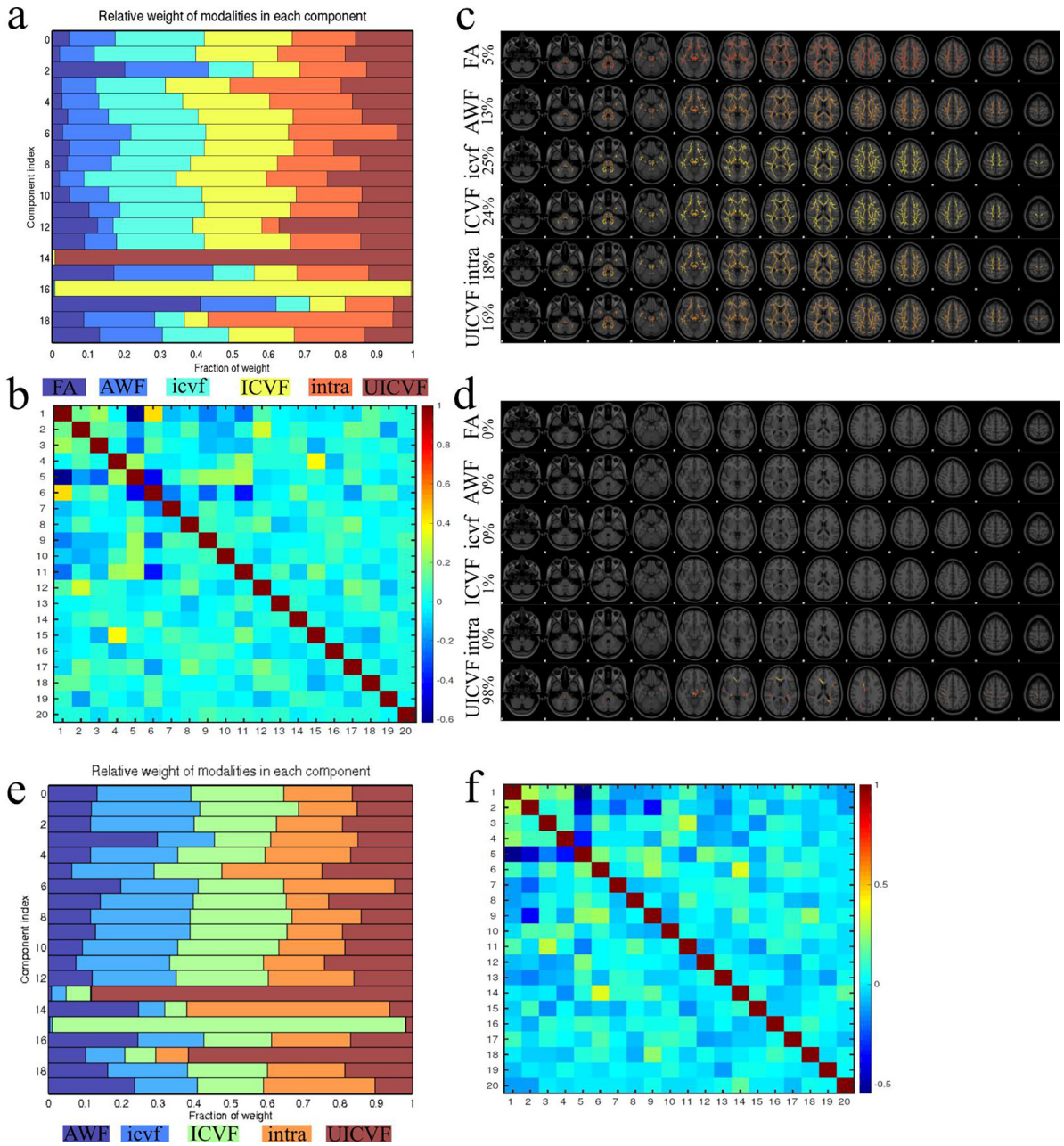

Figure 2. Results of LICA analysis based on diffusion metrics and TBSS skeleton with (a,c,d) and without (e,f) FA values. Number of independent components (IC) is equal to 20. a) contribution of diffusion metrics (x-axis: fraction of weight) into 20 IC (y-axis) including FA values; b) correlation map of weight coefficients for 20 IC with FA values; c) spatial patterns of common variance in the case of the first component; d) spatial patterns of common variance in the case of the 15th component; e) contribution of diffusion metrics (x-axis: fraction of weight) into 20 IC without FA values; f) correlation map of weight coefficients for 20 IC without FA values.

and ICVF groups, AWF and intra, and AWF, icvf and ICVF groups are the same.

Fig. 7 and Table 2 show results from the analysis testing for associations between age and AI for the different metrics. In brief, all AWF metrics showed decreasing AI with increasing age, i.e. less pronounced hemispheric asymmetry. In contrast, AI for FA showed positive associations with age. The highest R-squared and GLM slope values were found for *intra* and *UICVF* metrics. Cocor function [15] from R did not reveal any significant difference between all AI metrics.

Please cite this article as: I.I. Maximov and L.T. Westlye, Comparison of different neurite density metrics with brain asymmetry evaluation, Z Med Phys, https://doi.org/10.1016/j.zemedi.2023.07.003

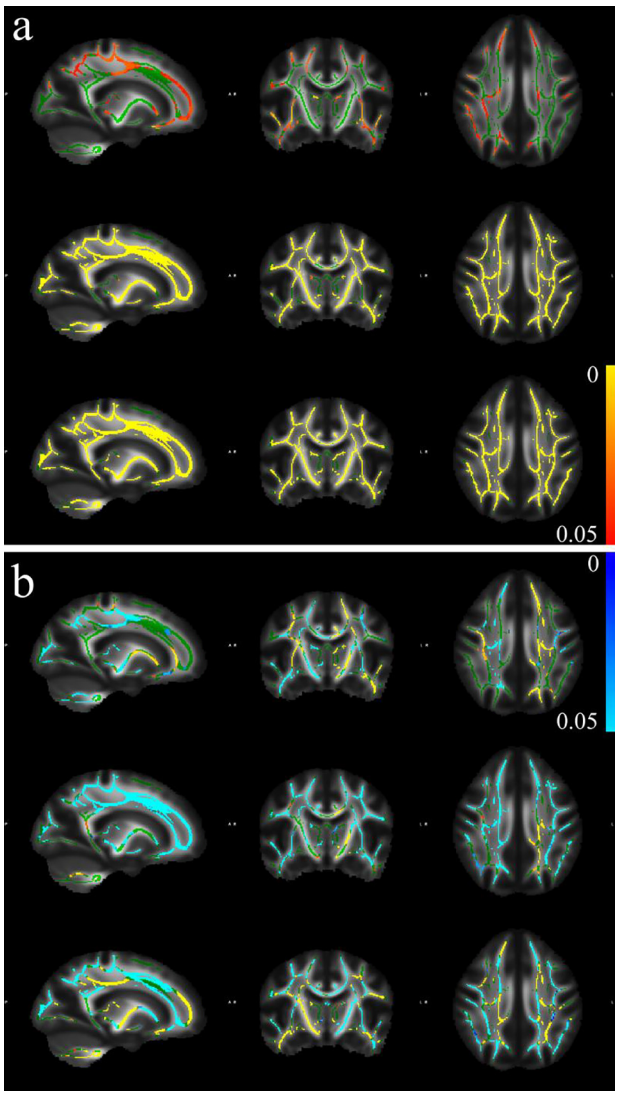

Figure 3. Voxelwise comparison of NODDI metrics using TBSS approach. The TBSS results are ordered as the following: the top row is AWF, the middle row is isotropic water fraction, and the bottom row is orientation distribution. The yellow-red colour marks the regions with values higher ($p < 0.05$) in subplot groups, the light blue-blue colour marks the regions with values lower ($p < 0.05$) in subplot groups. The skeleton is marked by the green colour. **a**) comparison of original NODDI metrics vs NODDI AMICO; **b**) comparison of NODDI AMICO metrics vs UKB NODDI AMICO.

Discussion

The diffusion parameters derived from the standard diffusion model [57,29] are limited by their non-linear estimation, numerical instability and being dependent on acquired image quality, e.g., affected by a low signal-to-noise ratio and applied imaging techniques such as EPI, concomitant eddy currents etc. Our comparison of different metrics reflecting intra-axonal water fraction obtained from WMTI, NODDI, and SMT demonstrated high correlations between averaged metrics, but also diverging findings related to brain asymmetry and its association with age. Further, comparison revealed significant voxel-wise differences in NODDI metrics between data assessed using different algorithms (original NODDI vs AMICO) or pre-processing pipeline (original UKB pipeline vs optimised pipeline). In particular, LICA demonstrated that the NODDI AMICO algorithm might affect the diffusion metrics introducing algorithm specific variances and an estimation of ICs. Similarly, the asymmetry index analysis derived from the different diffusion metrics revealed metric specific voxel-wise patterns and age associations. Notably, the means of AI are different for all diffusion metrics, however, exhibiting equal mean's pairs, for example, for icvf and ICVF.

Axonal water fraction as a proxy of neurite density can be estimated using different numerical algorithms with different theoretical assumptions in order to make the computations more reliable within the framework of the standard diffusion model, and the same biophysical feature can be estimated using different approaches such as WMTI, NODDI, and SMT. While different implementations of the same model, such as the original NODDI and NODDI AMICO, may produce different results, the mean skeleton diffusion metrics demonstrated high correlations overall. In contrast, the neurite density distribution demonstrated differences with modes around 0.59 for NODDI and SMT, and ∼0.51 for WMTI (see Fig. 1). Lower mode of AWF values in contrast to other diffusion approaches could be stipulated by not accurately satisfied WMTI assumptions over the whole skeleton. Indeed, not all skeleton regions could be treated as a coherent neurite bundle and the relationship between intra- and extra-axonal diffusivities chosen in WMTI seems to be not valid. As a result, the estimated neurite density metric for WMTI has lower value after skeleton averaging. Another reason for such behaviour is a different relationship between intra- and extra-axonal axial diffusivities used as practical assumptions in SMT/NODDI and WMTI models. This relationship might seriously affect the obtained solutions on a quite flat optimisation landscape (see, for example, similar results in Refs. [31,32,35,14].

LICA allowed us to decompose the various metrics as a linear mixture of independent spatial components and identify spatial patterns with common and unique variance and to estimate the relative contribution of each modality to each component. Assuming that the different metrics all represent the same biophysical property, we expected to see a high degree of fusing across all neurite density metrics. As expected, the primary independent components, which explain the largest amount of the total variance, were highly multimodal with contributions from all metrics maps (see,

Please cite this article as: I.I. Maximov and L.T. Westlye, Comparison of different neurite density metrics with brain asymmetry evaluation, Z Med Phys, https://doi.org/10.1016/j.zemedi.2023.07.003

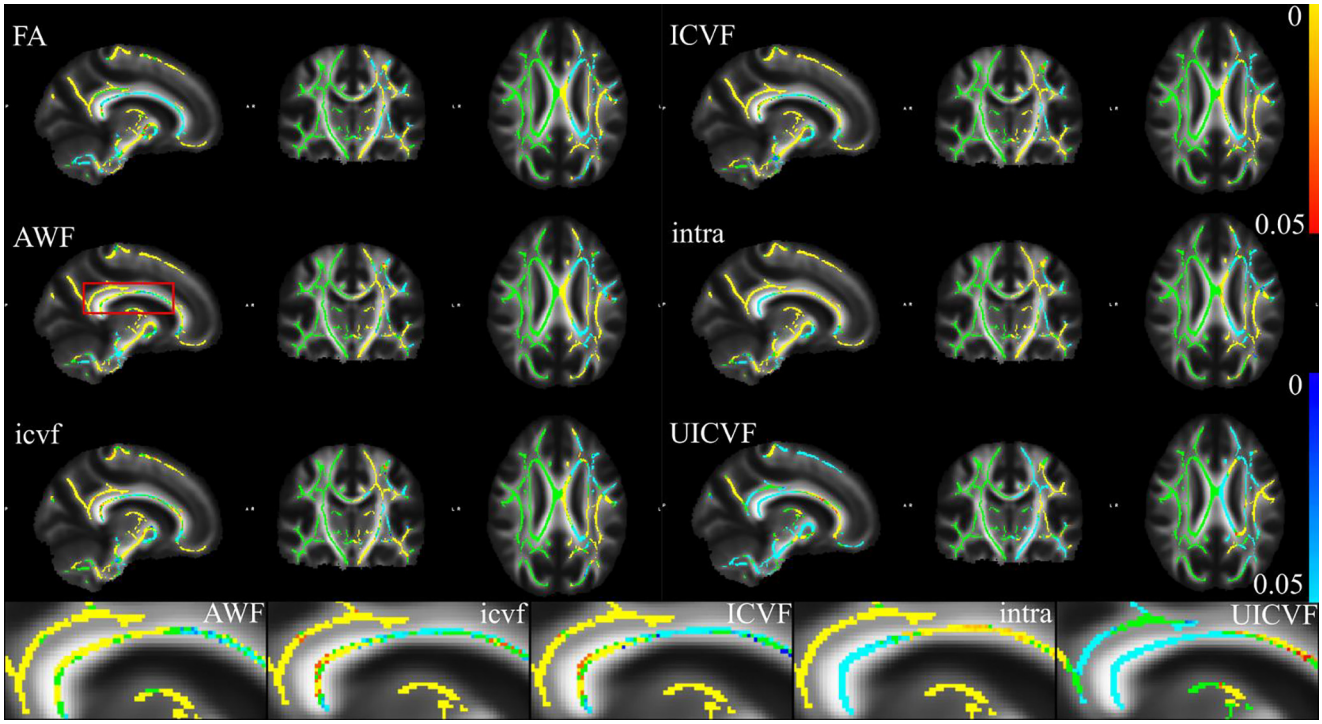

Figure 4. The result of TBSS analysis using the brain asymmetry feature. Diffusion metrics are represented by FA and axonal water fractions from different diffusion models. The yellow-red colour marks the regions with values higher ($p < 0.05$) in the left hemisphere, the light blue-blue colour marks the regions with values lower ($p < 0.05$) in the left hemisphere. The bottom row shows enlarged images localised by the red frame at AWF map. The symmetrised skeleton is marked by the green colour.

Table 1
A comparison of spatial patterns obtained by TBSS asymmetry analysis ($p < 0.05$). In upper diagonal cells we present pairwise SSIM estimations between the skeleton regions with significant differences. In bottom diagonal cells we present the pairwise ratio of voxel numbers N: $(N_A \cap N_B)/N_A$, where $N_{A,B}$ is the number of voxel with significant difference from metrics A or B.

Values in the left hemisphere higher than in the right hemisphere					
	AWF	**intra**	**icvf**	**ICVF**	**UICVF**
AWF	1	0.9824	0.9819	0.9823	0.9608
intra	0.7809	1	0.9852	0.9860	0.9616
icvf	0.8017	0.8699	1	0.9972	0.9616
ICVF	0.8076	0.8797	0.9777	1	0.9614
UICVF	0.2068	0.1857	0.1850	0.1837	1
Values in the left hemisphere lower than in the right hemisphere					
	AWF	**intra**	**icvf**	**ICVF**	**UICVF**
AWF	1	0.9808	0.9804	0.9808	0.9605
intra	0.6006	1	0.9849	0.9857	0.9616
icvf	0.5483	0.6712	1	0.9968	0.9605
ICVF	0.5619	0.6956	0.9718	1	0.9604
UICVF	0.4151	0.4505	0.3530	0.3576	1

for example, at first 4 ICs in Fig 2a,e). However, several ICs were also dominated by one or few metrics, in particular *ICVF* and *UICVF,* suggesting unique variance in the NODDI AMICO maps that was not captured in the original NODDI implementation. While the total amount of variance explained by these spatial patterns defined by *UICVF* or *ICVF* is relatively small, they might create spurious findings in the downstream analysis [16,23,24]. It is particularly interesting finding, because allows us to suppose a presence of unique features in ICVF and UICVF maps independently

Please cite this article as: I.I. Maximov and L.T. Westlye, Comparison of different neurite density metrics with brain asymmetry evaluation, Z Med Phys, https://doi.org/10.1016/j.zemedi.2023.07.003

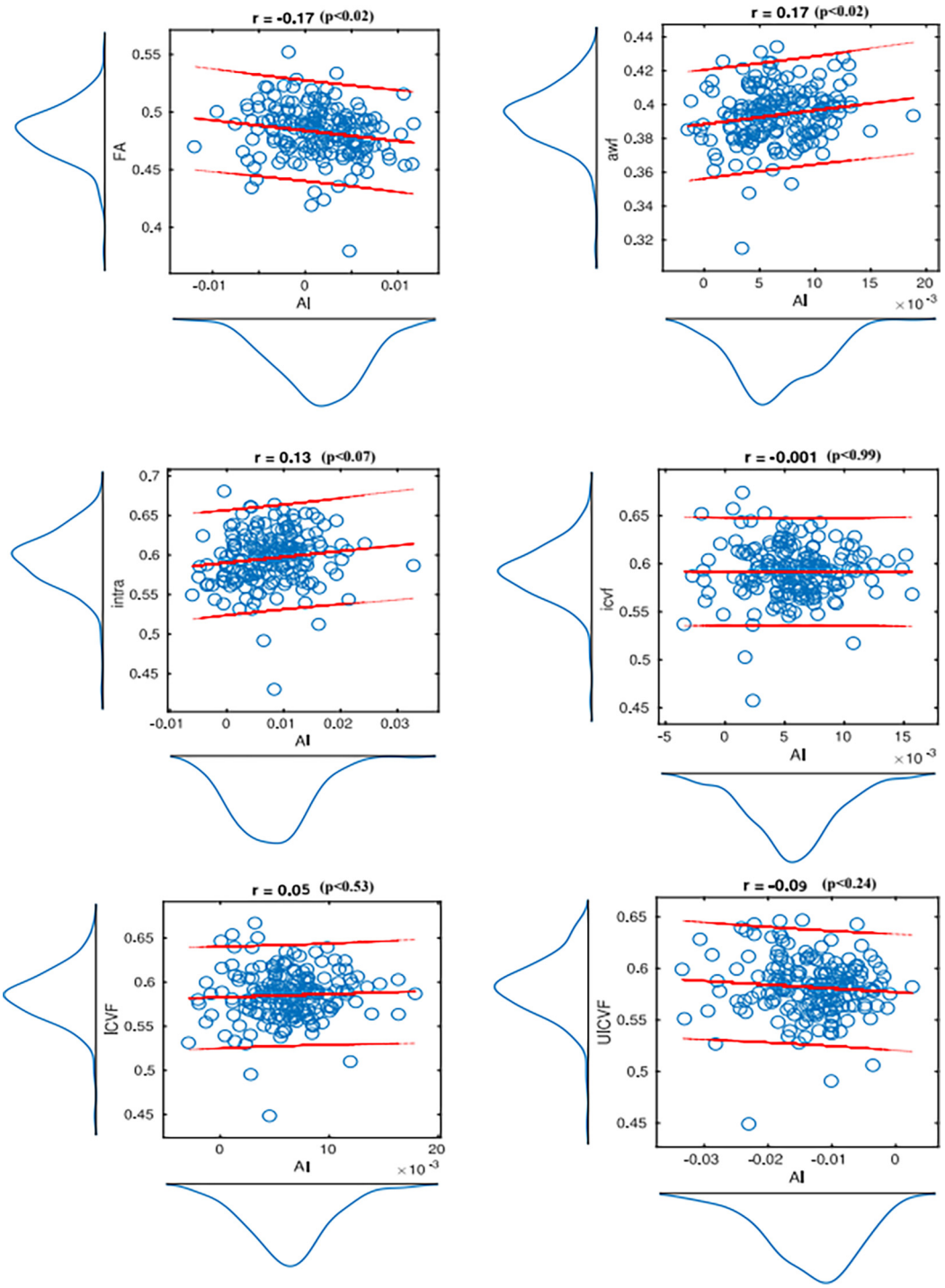

Figure 5. The result of linear regression of diffusion metrics and their derived AI. The red lines are linear regression fit and intervals of confidence (95%). The Pearson correlation coefficients are presented on the top of each correlation plot.

on the used post-processing pipeline, i.e. unique only for NODDI AMICO approach.

Hence, the LICA findings indicate some inconsistencies in the derived metrics from the two NODDI implementations. The voxel-wise TBSS analysis revealed that the UKB pipeline and the optimised [51] processing pipelines influenced NODDI AMICO metrics, which for isotropic water faction and orientation dispersion covered almost all skeleton voxels and for intra-axonal water fraction showed more complex patterns with both higher and lower values.

Please cite this article as: I.I. Maximov and L.T. Westlye, Comparison of different neurite density metrics with brain asymmetry evaluation, Z Med Phys, https://doi.org/10.1016/j.zemedi.2023.07.003

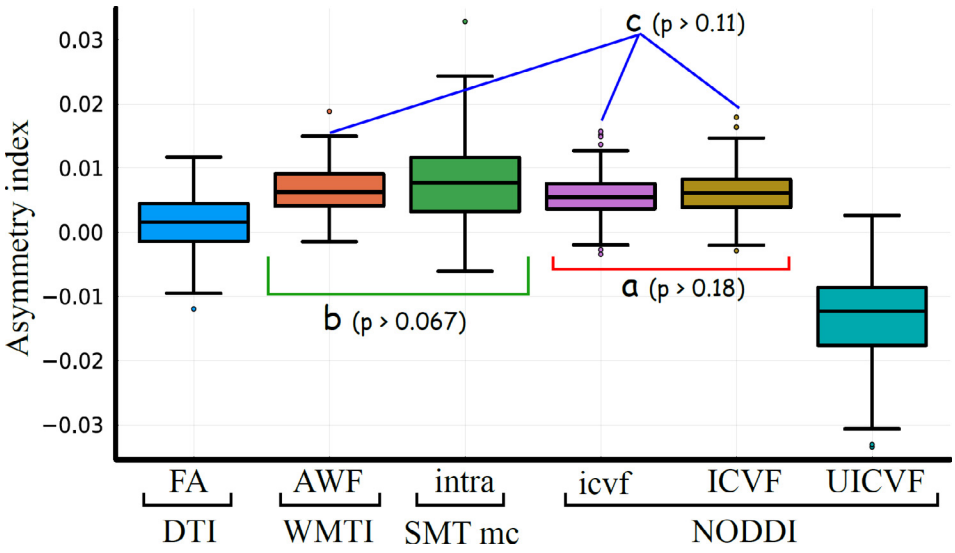

Figure 6. Boxplots of asymmetry index derived from the different diffusion metrics. All AI means are different including and excluding FA values in accordance with a Kruskal-Wallis test. Three groups, obtained from post hoc analysis, have the equal AI means: **a**) original and AMICO NODDI; **b**) WMTI and SMT mc metrics; and **c**) WMTI, original and AMICO NODDI metrics. *P*-values are presented for supporting H_0 hypothesis (all means are equal).

These findings emphasise the need for harmonised and careful considerations of the different steps in the data processing, cleaning and analysis, including noise correction [1] and the exact numerical implementation of the diffusion approaches [13,52].

Although the diffusion metrics reflect important microstructure brain features on their own, it can be used for a description of macroscale brain architecture such as brain asymmetry [17]. Brain asymmetry is a basic feature of brain organisation and the asymmetry index represents a potentially useful imaging based biomarker [89], e.g. in relation to brain development and aging [73,76,5] and mental disorders [39,84]. The AI values based on different diffusion approaches and conventional FA using symmetrised TBSS skeleton revealed some inconsistencies in the results produced by the different metrics, in particular, for *UICVF* (see Fig. 4).

The correlation between the mean skeleton metrics and their corresponding AI was negligible for *icvf*, *ICVF*, and *UICVF*, and low for FA, *AWF*, and *intra* metrics. While the correlations were low, *icvf* and *UICVF* metrics exhibited correlations with opposite signs. These results showed that AI represent an imaging derived phenotype that is largely independent from the overall value of the corresponding metric. Importantly, the mean AI metrics are different derived from all axonal water fraction approaches.

Linear models revealed similar associations with age for all neurite density metrics, and we found no significant differences in the slopes between metrics. The low regression slope for FA partially reproduces previous results [86]. The associations between global AI and age were overall weak, suggesting no dramatic age-related differences in brain asymmetry in the sampled age range. In order to validate this finding and to increase the statistical power in future work, we plan to perform a more accurate analysis of brain asymmetry using a larger portion of the UKB data with regional parcellation [53]. In accordance with our experience, the averaged diffusion metrics associated with AI might be less sensitive markers in contrast to the voxel-wise or region-of-interest methods of analysis [45]. In turn, it stimulates an application of the advanced methods of analysis such as deep learning networks or FEMA (Parekh et al., 2023).

Some methodological considerations are worth mentioning. In contrast to the assumptions in WMTI, NODDI, and SMT, recent results suggest that intra-axonal diffusivity is higher than extra-axonal diffusion [14,35,46,27]. Thus, an alternative implementation of the standard diffusion model, for instance, WMTI modification suggested by Jespersen and colleagues, 2018, should be superior. Future work should evaluate such approaches in large population cohorts (see, for example [45]). In turn, recent results in artefact correction and development of pre-processing pipeline [1,55] should bring higher accuracy in the statistical analysis. For example, the used step such as smoothing with the Gaussian kernel equals to half of spatial resolution improved numerical estimations in many diffusion approaches, in particular, in DKI and NODDI. Although, the spatial smoothing

Please cite this article as: I.I. Maximov and L.T. Westlye, Comparison of different neurite density metrics with brain asymmetry evaluation, Z Med Phys, https://doi.org/10.1016/j.zemedi.2023.07.003

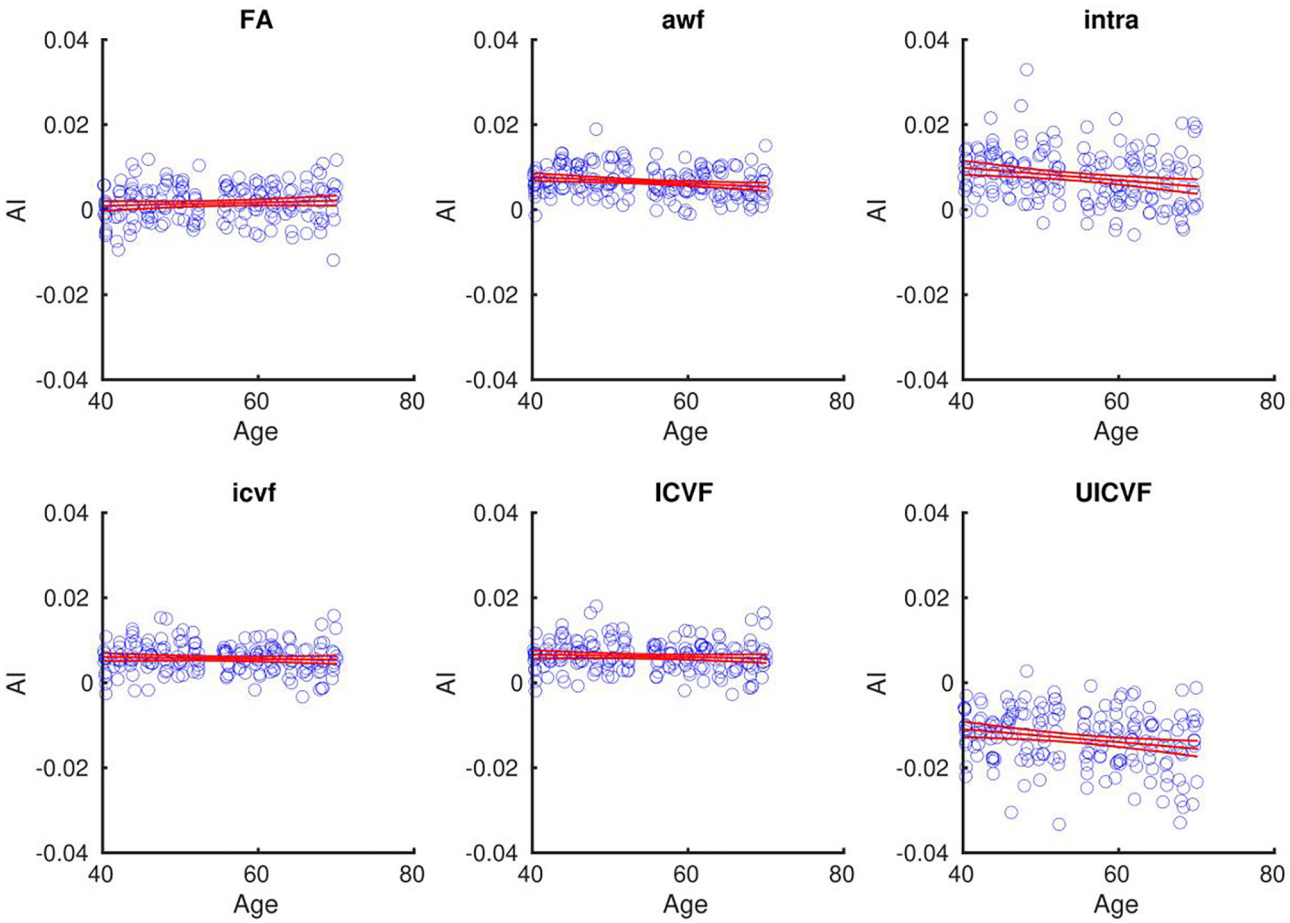

Figure 7. The results of GLM fit of age and AI dependencies. The parameters of GLM fits are presented in Tab. 2. The red lines are linear regression fit and interval of confidence (CI = 95%).

Table 2
Parameters of regression fits for AI dependence on age using different diffusion metrics (see Fig. 6). The GLM is AI = $b_0 + b_1$ Age + b_2 Sex. RMSE is the root mean squared error, R-squared is the coefficient of determination, CI is the confidence interval. Coefficients b_0/b_1 significantly different from zero ($p < 0.05$) are marked by red bold font.

	Intercept, b_0 [CI]	**Slope**, b_1 [CI]	**RMSE**	**R-squared**	**F-statistics**
FA	$-7.6880 \cdot 10^{-4}$ $[-4.4; 2.9] \cdot 10^{-3}$	$4.1383 \cdot 10^{-5}$ $[0; 1] \cdot 10^{-3}$	0.0042	0.0207	1.89
AWF	**0.0108** [0.0078; 0.0138]	$\mathbf{-7.7402 \cdot 10^{-5}}$ $[-1; 0] \cdot 10^{-3}$	0.0035	0.0427	3.99
intra	**0.0157** [0.0105; 0.0210]	$\mathbf{-1.4689 \cdot 10^{-4}}$ $[-2; -1] \cdot 10^{-4}$	0.0060	0.0512	4.83
icvf	**0.0069** [0.0039; 0.0099]	$-2.2013 \cdot 10^{-5}$ $[-1; 0] \cdot 10^{-4}$	0.0035	0.0036	0.32
ICVF	**0.0080** [0.0048; 0.0111]	$-3.2509 \cdot 10^{-5}$ $[-1; 0] \cdot 10^{-4}$	0.0036	0.0071	0.63
UICVF	−0.0049 [−0.0106; 0.0009]	$\mathbf{-1.5223 \cdot 10^{-4}}$ $[-3; 0] \cdot 10^{-4}$	0.0066	0.0504	4.75

Please cite this article as: I.I. Maximov and L.T. Westlye, Comparison of different neurite density metrics with brain asymmetry evaluation, Z Med Phys, https://doi.org/10.1016/j.zemedi.2023.07.003

brought slightly negative effect such as image blurring which is not very important in the case of skeleton analysis as we already demonstrated in [51,53]. Nevertheless, we hope that new developing approaches in diffusion artefact clearance would avoid demands for any kind of smoothing steps in the future.

In conclusion, our analysis suggests that NODDI scalar metrics are dependent on numerical algorithm and post-processing pipeline. The AWF metrics derived from the standard diffusion model are different and depending on the used assumptions, in particular, in the case of NODDI AMICO approach as revealed by LICA analysis. In turn, a reproducibility of NODDI metrics should be considered very carefully, in particular, in a consequential statistics, even after an application of proxy measures such as AI. We found that the brain asymmetry derived from neurite density metrics represents a potentially useful biomarker that can be used as an additional imaging based phenotype, in particular, for brain aging studies due to decreasing AI along the ageing.

Data availability statement

The data that supports the findings of this study are available throught UK Biobank data access procedures (https://www.ukbiobank.ac.uk/researchers).

Declaration of Competing Interest

The authors declare that they have no known competing financial interests or personal relationships that could have appeared to influence the work reported in this paper.

Acknowledgment

This work was funded by the Research Council of Norway (249795). This research has been conducted using the UK Biobank under Application 27412.

Appendix A Supplementary data

Supplementary data to this article can be found online at https://doi.org/10.1016/j.zemedi.2023.07.003.

References

[1] Ades-Aron B, Veraart J, Kochunov P, McGuire S, Sherman P, Kellner E, Novikov DS, Fieremans E. Evaluation of the accuracy and precision of the diffusion parameter EStImation with Gibbs and NoisE removal pipeline. Neuroimage 2018;183:532–543.

[2] Alfaro-Almagro F, Jenkinson M, Bangerter NK, Andersson JLR, Griffanti L, Douaud G, Sotiropoulos SN, Jbabdi S, Hernandez-Fernandez M, Vallee E, Vidaurre D, Webster M, McCarthy P, Rorden C, Daducci A, Alexander DC, Zhang H, Dragonu I, Matthews PM, Miller KL, Smith SM. Image processing and Quality Control for the first 10,000 brain imaging datasets from UK Biobank. NeuroImage 2018;166:400–424. https://doi.org/10.1016/j.neuroimage.2017.10.034.

[3] Andersson JLR, Graham MS, Zsoldos E, Sotiropoulos SN. Incorporating outlier detection and replacement into a non-parametric framework for movement and distortion correction of diffusion MR images. NeuroImage 2016;141:556–572. https://doi.org/10.1016/j.neuroimage.2016.06.058.

[4] Andersson JLR, Sotiropoulos SN. An integrated approach to correction for off-resonance effects and subject movement in diffusion MR imaging. NeuroImage 2016;125:1063–1078. https://doi.org/10.1016/j.neuroimage.2015.10.019.

[5] Arun AH, Connelly A, Smith RE, Calamante F. Characterisation of white matter asymmetries in the healthy human brain using diffusion MRI fixel-based analysis. Neuroimage 2021;225:117505. https://doi.org/10.1016/j.neuroimage.2020.117505.

[6] Assaf Y, Basser PJ. Composite hindered and restricted model of diffusion (CHARMED) MR imaging of the human brain. NeuroImage 2005;27:48–58. https://doi.org/10.1016/j.neuroimage.2005.03.042.

[7] Assaf Y, Blumenfeld-Katzir T, Yovel Y, Basser PJ. Axcaliber: A method for measuring axon diameter distribution from diffusion MRI. Magn Reson Med 2008;59:1347–1354. https://doi.org/10.1002/mrm.21577.

[8] Basser PJ, Mattiello J, Lebihan D. Estimation of the Effective Self-Diffusion Tensor from the NMR Spin Echo. J Magn Reson B 1994;103:247–254. https://doi.org/10.1006/jmrb.1994.1037.

[9] Beck D, de Lange A-M, Maximov II, Richard G, Andreassen OA, Nordvik JE, Westlye LT. White matter microstructure across the adult lifespan: a mixed longitudinal and cross-sectional study using advanced diffusion models and brain-age prediction. Neuroimage 2021;224:117441. https://doi.org/10.1016/j.neuroimage.2020.117441.

[10] Bennett KM, Schmainda KM, Bennett RT, Rowe DB, Lu H, Hyde JS. Characterization of continuously distributed cortical water diffusion rates with a stretched-exponential model. Magn Reson Med 2003;50:727–734. https://doi.org/10.1002/mrm.10581.

[11] Coelho S, Pozo JM, Jespersen SN, Jones DK, Frangi AF. Resolving degeneracy in diffusion MRI biophysical model parameter estimation using double diffusion encoding. Magn Reson Med 2019;82:395–410. https://doi.org/10.1002/mrm.27714.

[12] Daducci A, Canales-Rodríguez EJ, Zhang H, Dyrby TB, Alexander DC, Thiran J-P. Accelerated Microstructure Imaging via Convex Optimization (AMICO) from diffusion MRI data. NeuroImage 2015;105:32–44. https://doi.org/10.1016/j.neuroimage.2014.10.026.

[13] David S, Mesri HY, Viergever MA, Leemans A. Statistical significance in DTI group analyses: How the choice of the estimator can inflate effect sizes. bioRxiv 2019. https://doi.org/10.1101/755140.

[14] Dhital B, Reisert M, Kellner E, Kiselev VG. Intra-axonal diffusivity in brain white matter. Neuroimage 2019;189:543–550. https://doi.org/10.1016/j.neuroimage.2019.01.015.

[15] Didenhofen D, Musch J. cocor: A Comprehensive Solution for the Statistical Comparison of Correlations. PLOS One 2015;0121945. https://doi.org/10.1371/journal.pone.0121945.

[16] Doan NT, Engvig A, Persson K, Alnæs D, Kaufmann T, Rokicki J, Córdova-Palomera A, Moberget T, Brækhus A, Barca ML, Engedal K, Andreassen OA, Selbæk G, Westlye LT. Dissociable diffusion MRI patterns of white matter microstructure and connectivity in

Please cite this article as: I.I. Maximov and L.T. Westlye, Comparison of different neurite density metrics with brain asymmetry evaluation, Z Med Phys, https://doi.org/10.1016/j.zemedi.2023.07.003

Alzheimer's disease spectrum. Sci Rep 2017;7:45131. https://doi.org/10.1038/srep45131.

[17] Duboc V, Dufourcq P, Blader P, Roussigné M. Asymmetry of the Brain: Development and Implications. Annu Rev Genet 2015;49:647–672. https://doi.org/10.1146/annurev-genet-112414-055322.

[18] Eed A, Cerda AC, Lerma J, De Santis S. Diffusion-weighted MRI in neurodegenerative and psychiatric animal models: experimental strategies and main outcomes. J Neurosci Methods 2020;343:108814. https://doi.org/10.1016/j.jneumeth.2020.108814.

[19] Elliott LT, Sharp K, Alfaro-Almagro F, Shi S, Miller KL, Douaud G, Marchini J, Smith SM. Genome-wide association studies of brain imaging phenotypes in UK Biobank. Nature 2018;562:210–216. https://doi.org/10.1038/s41586-018-0571-7.

[20] Fan Q, Tian Q, Ohringer NA, Nummenmaa A, Witzel T, Tobyne SM, Klawiter EC, Mekkaoui C, Rosen BR, Wald LL, Salat DH, Huang SY. Age-related alterations in axonal microstructure in the corpus callosum measured by high-gradient diffusion MRI. Neuroimage 2019;191:325–336. https://doi.org/10.1016/j.neuroimage.2019.02.036.

[21] Fieremans E, Jensen JH, Helpern JA. White matter characterization with diffusional kurtosis imaging. NeuroImage 2011;58:177–188. https://doi.org/10.1016/j.neuroimage.2011.06.006.

[22] Fieremans E, Lee H-H. Physical and numerical phantoms for the validation of brain microstructural MRI: A cookbook. NeuroImage 2018;182:39–61. https://doi.org/10.1016/j.neuroimage.2018.06.046.

[23] Groves AR, Beckmann CF, Smith SM, Woolrich MW. Linked independent component analysis for multimodal data fusion. NeuroImage 2011;54:2198–2217. https://doi.org/10.1016/j.neuroimage.2010.09.073.

[24] Groves AR, Smith SM, Fjell AM, Tamnes CK, Walhovd KB, Douaud G, Woolrich MW, Westlye LT. Benefits of multi-modal fusion analysis on a large-scale dataset: life-span patterns of inter-subject variability in cortical morphometry and white matter microstructure. Neuroimage 2012;63:365–380. https://doi.org/10.1016/j.neuroimage.2012.06.038.

[25] Grussu F, Schneider T, Tur C, Yates RL, Tachrount M, Ianuş A, Yiannakas MC, Newcombe J, Zhang H, Alexander DC, DeLuca GC, Gandini Wheeler-Kingshott CAM. Neurite dispersion: a new marker of multiple sclerosis spinal cord pathology?. Ann Clin Transl Neurol 2017;4:663–679. https://doi-org.ezproxy.uio.no/10.1002/acn3.445.

[26] Henriques RN, Jespersen SN, Shemesh N. Microscopic anisotropy misestimation in spherical-mean single diffusion encoding MRI. Magn Reson Med 2019;81:3245–3261. https://doi.org/10.1002/mrm.27606.

[27] Howard AFD, Cottaar M, Drakesmith M, Fan Q, Huang SY, Jones DK, Lange FJ, Mollink J, Rudrapatna SU, Tian Q, Miller KL, Jbabdi S. Estimating axial diffusivity in the NODDI model. Neuroimage 2022;262:119535. https://doi.org/10.1016/j.neuroimage.2022.119535.

[28] Ianuş A, Jespersen SN, Serradas Duarte T, Alexander DC, Drobnjak I, Shemesh N. Accurate estimation of microscopic diffusion anisotropy and its time dependence in the mouse brain. NeuroImage 2018;183:934–949. https://doi.org/10.1016/j.neuroimage.2018.08.034.

[29] Jelescu IO, Budde MD. Design and Validation of Diffusion MRI Models of White Matter. Front Phys 2017;5. https://doi.org/10.3389/fphy.2017.00061.

[30] Jelescu IO, Palombo M, Bagnato F, Schilling KG. Challenges for biophysical modeling of microstructure. J Neurosci Methods 2020;344:108861. https://doi.org/10.1016/j.jneumeth.2020.108861.

[31] Jelescu IO, Veraart J, Adisetiyo V, Milla SS, Novikov DS, Fieremans E. One diffusion acquisition and different white matter models: How does microstructure change in human early development based on WMTI and NODDI? NeuroImage 2015;107:242–256. https://doi.org/10.1016/j.neuroimage.2014.12.009.

[32] Jelescu IO, Veraart J, Fieremans E, Novikov DS. Degeneracy in model parameter estimation for multi-compartmental diffusion in neuronal tissue: Degeneracy in Model Parameter Estimation of Diffusion in Neural Tissue. NMR Biomed 2016;29:33–47. https://doi.org/10.1002/nbm.3450.

[33] Jensen JH, Helpern JA, Ramani A, Lu HZ, Kaczynski K. Diffusional kurtosis imaging: The quantification of non-Gaussian water diffusion by means of magnetic resonance imaging. Magn Res Med 2005;53:1432–1440. https://doi.org/10.1002/mrm.20508.

[34] Jespersen SN, Bjarkam CR, Nyengaard JR, Chakravarty MM, Hansen B, Vosegaard T, Østergaard L, Yablonskiy D, Nielsen NC, Vestergaard-Poulsen P. Neurite density from magnetic resonance diffusion measurements at ultrahigh field: Comparison with light microscopy and electron microscopy. Neuroimage 2010;49:205–216. https://doi.org/10.1016/j.neuroimage.2009.08.053.

[35] Jespersen SN, Olesen JL, Hansen B, Shemesh N. Diffusion time dependence of microstructural parameters in fixed spinal cord. Neuroimage 2018;182:329–342. https://doi.org/10.1016/j.neuroimage.2017.08.039.

[36] Jespersen SN, Olesen JL, Ianuş A, Shemesh N. Effects of nongaussian diffusion on "isotropic diffusion" measurements: An ex-vivo microimaging and simulation study. J Magn Reson 2019;300:84–94. https://doi.org/10.1016/j.jmr.2019.01.007.

[37] Johansen-Berg H, Behrens TEJ. Diffusion MRI: from quantitative measurement to in-vivo neuroanatomy. 2nd ed. London, UK; Waltham, MA: Elsevier/Academic Press; 2014.

[38] Jones DK. Diffusion MRI: theory, methods, and application. Oxford, New York: Oxford University Press; 2010.

[39] Joo SW, Chon M-W, Rathi Y, Shenton ME, Kubicki M, Lee J. Abnormal asymmetry of white matter tracts between ventral posterior cingulate cortex and middle temporal gyrus in recent-onset schizophrenia. Schizophr Res 2018;192:159–166. https://doi.org/10.1016/j.schres.2017.05.008.

[40] Kaden E, Kelm ND, Carson RP, Does MD, Alexander DC. Multi-compartment microscopic diffusion imaging. NeuroImage 2016;139:346–359. https://doi.org/10.1016/j.neuroimage.2016.06.002.

[41] Kaden E, Kruggel F, Alexander DC. Quantitative mapping of the per-axon diffusion coefficients in brain white matter: Quantitative Mapping of the Per-Axon Diffusion Coefficients. Magn Reson Med 2016;75:1752–1763. https://doi.org/10.1002/mrm.25734.

[42] Kaufmann T, van der Meer D, Doan NT, Schwarz E, Lund MJ, Agartz I, Alnæs D, Barch DM, Baur-Streubel R, Bertolino A, Bettella F, Beyer MK, Bøen E, Borgwardt S, Brandt CL, Buitelaar J, Celius EG, Cervenka S, Conzelmann A, Córdova-Palomera A, Dale AM, de Quervain DJF, Carlo P, Djurovic S, Dørum ES, Eisenacher S, Elvsåshagen T, Espeseth T, Fatouros-Bergman H, Flyckt L, Franke B, Frei O, Haatveit B, Håberg AK, Harbo HF, Hartman CA, Heslenfeld D, Hoekstra PJ, Høgestøl EA, Jernigan TL, Jonassen R, Jönsson EG, Kirsch P, Kłoszewska I, Kolskår KK, Landrø NI, Hellard S, Lesch K-P, Lovestone S, Lundervold A, Lundervold AJ, Maglanoc LA, Malt UF, Mecocci P, Melle I, Meyer-Lindenberg A, Moberget T, Norbom LB, Nordvik JE, Nyberg L, Oosterlaan J, Papalino M, Papassotiropoulos A, Pauli P, Pergola G, Persson K, Richard G, Rokicki J, Sanders A-M, Selbæk G, Shadrin AA, Smeland OB, Soininen H, Sowa P, Steen VM, Tsolaki M, Ulrichsen KM, Vellas B, Wang L, Westman E, Ziegler GC, Zink M, Andreassen OA, Westlye LT. Common brain disorders are associated with heritable patterns of apparent aging of the brain.

Please cite this article as: I.I. Maximov and L.T. Westlye, Comparison of different neurite density metrics with brain asymmetry evaluation, Z Med Phys, https://doi.org/10.1016/j.zemedi.2023.07.003

Nat Neurosci 2019;22:1617–1623. https://doi.org/10.1038/s41593-019-0471-7.

[43] Kellner E, Dhital B, Kiselev VG, Reisert M. Gibbs-ringing artifact removal based on local subvoxel-shifts: Gibbs-Ringing Artifact Removal. Magn Reson Med 2016;76:1574–1581. https://doi.org/10.1002/mrm.26054.

[44] Komlosh ME, Benjamini D, Barnett AS, Schram V, Horkay F, Avram AV, Basser PJ. Anisotropic phantom to calibrate high-q diffusion MRI methods. J Magn Reson 2017;275:19–28. https://doi.org/10.1016/j.jmr.2016.11.017.

[45] Korbmacher M, Gurholt TP, de Lange AM, van der Meer D, Beck D, Eikefjord E, Lundervold A, Andreassen OA, Westlye LT, Maximov II. Bio-psycho-social factors' associations with brain age: a large-scale UK Biobank diffusion study of 35,749 participants. Front. Psychol. 2023;14:1117732. https://doi.org/10.1101/2022.12.12.22283360.

[46] Kunz N, da Silva AR, Jelescu IO. Intra- and extra-axonal axial diffusivities in the white matter: Which one is faster? Neuroimage 2018;181:314–322. https://doi.org/10.1016/j.neuroimage.2018.07.020.

[47] Lampinen B, Szczepankiewicz F, Mårtensson J, van Westen D, Sundgren PC, Nilsson M. Neurite density imaging versus imaging of microscopic anisotropy in diffusion MRI: A model comparison using spherical tensor encoding. NeuroImage 2017;147:517–531. https://doi.org/10.1016/j.neuroimage.2016.11.053.

[48] Lampinen B, Szczepankiewicz F, Novén M, Westen D, Hansson O, Englund E, Mårtensson J, Westin C, Nilsson M. Searching for the neurite density with diffusion MRI: Challenges for biophysical modeling. Hum Brain Mapp 2019;40:2529–2545. https://doi.org/10.1002/hbm.24542.

[49] Lee H-H, Yaros K, Veraart J, Pathan JL, Liang F-X, Kim SG, Novikov DS, Fieremans E. Along-axon diameter variation and axonal orientation dispersion revealed with 3D electron microscopy: implications for quantifying brain white matter microstructure with histology and diffusion MRI. Brain Struct Funct 2019;224:1469–1488. https://doi.org/10.1007/s00429-019-01844-6.

[50] Lemberskiy G, Baete SH, Cloos MA, Novikov DS, Fieremans E. Validation of surface-to-volume ratio measurements derived from oscillating gradient spin echo on a clinical scanner using anisotropic fiber phantoms. NMR Biomed 2017;30:e3708.

[51] Maximov II, Alnæs D, Westlye LT. Towards an optimised processing pipeline for diffusion magnetic resonance imaging data: Effects of artefact corrections on diffusion metrics and their age associations in UK Biobank. Human Brain Mapping 2019;40:4146–4162. https://doi.org/10.1002/hbm.24691.

[52] Maximov II, Thönneßen H, Konrad K, Amort L, Neuner I, Shah NJ. Statistical Instability of TBSS Analysis Based on DTI Fitting Algorithm: TBSS analysis. J Neuroimaging 2015;25:883–891. https://doi.org/10.1111/jon.12215.

[53] Maximov II, van der Meer D, de Lange A-M, Kaufmann T, Shadrin A, Frei O, Wolfers T, Westlye LT. Fast qualit **Y** con **T** rol me **T** hod fo **R** der **I** ved diff **U** sion **M** etrics (**YTTRIUM**) in big data analysis: UK Biobank 18608 example. Human Brain Mapping 2021;42:3141–3155. https://doi.org/10.1002/hbm.25424.

[54] Miller KL, Alfaro-Almagro F, Bangerter NK, Thomas DL, Yacoub E, Xu J, Bartsch AJ, Jbabdi S, Sotiropoulos SN, Andersson JLR, Griffanti L, Douaud G, Okell TW, Weale P, Dragonu I, Garratt S, Hudson S, Collins R, Jenkinson M, Matthews PM, Smith SM. Multimodal population brain imaging in the UK Biobank prospective epidemiological study. Nat Neurosci 2016;19:1523–1536. https://doi.org/10.1038/nn.4393.

[55] Muckley MJ, Ades-Aron B, Papaioannou A, Lemberskiy G, Solomon E, Lui YW, Sodickson DK, Fieremans E, Novikov DS, Knoll F. Training a neural network for Gibbs and noise removal in diffusion MRI. Magn Reson Med 2021;85:413–428. https://doi.org/10.1002/mrm.28395.

[56] Neilson E, Shen X, Cox SR, Clarke T-K, Wigmore EM, Gibson J, Howard DM, Adams MJ, Harris MA, Davies G, Deary IJ, Whalley HC, McIntosh AM, Lawrie SM. Impact of Polygenic Risk for Schizophrenia on Cortical Structure in UK Biobank. Biol Psychiatry 2019. https://doi.org/10.1016/j.biopsych.2019.04.013.

[57] Novikov DS, Fieremans E, Jespersen SN, Kiselev VG. Quantifying brain microstructure with diffusion MRI: Theory and parameter estimation. NMR Biomed 2019;32:e3998.

[58] Novikov DS, Kiselev VG, Jespersen SN. On modeling. Magn Reson Med 2018;79:3172–3193. https://doi.org/10.1002/mrm.27101.

[59] Novikov DS, Veraart J, Jelescu IO, Fieremans E. Rotationally-invariant mapping of scalar and orientational metrics of neuronal microstructure with diffusion MRI. NeuroImage 2018;174:518–538. https://doi.org/10.1016/j.neuroimage.2018.03.006.

[60] Petiet A. Current and Emerging MR Methods and Outcome in Rodent Models of Parkinson's Disease: a review. Front Neurosci 2021;15:583678. https://doi.org/10.3389/fnins.2021.583678.

[61] Ratnarajah N, Rifkin-Graboi A, Fortier MV, Chong YS, Kwek K, Saw SM, Godfrey KM, Gluckman PD, Meaney MJ, Qiu A. Structural connectivity asymmetry in the neonatal brain. Neuroimage 2013;75:187–194. https://doi.org/10.1016/j.neuroimage.2013.02.052.

[62] Ray KL, McKay DR, Fox PM, Riedel MC, Uecker AM, Beckmann CF, Smith SM, Fox PT, Laird AR. ICA model order selection of task co-activation networks. Front Neurosci 2013;7. https://doi.org/10.3389/fnins.2013.00237.

[63] Reisert M, Kiselev VG, Dhital B. A unique analytical solution of the white matter standard model using linear and planar encodings. Magn Reson Med 2019;81:3819–3825. https://doi.org/10.1002/mrm.27685.

[64] Roalf DR, Quarmley M, Elliott MA, Satterthwaite TD, Vandekar SN, Ruparel K, Gennatas ED, Calkins ME, Moore TM, Hopson R, Prabhakaran K, Jackson CT, Verma R, Hakonarson H, Gur RC, Gur RE. The impact of quality assurance assessment on diffusion tensor imaging outcomes in a large-scale population-based cohort. NeuroImage 2016;125:903–919. https://doi.org/10.1016/j.neuroimage.2015.10.068.

[65] Schilling KG, Janve V, Gao Y, Stepniewska I, Landman BA, Anderson AW. Histological validation of diffusion MRI fiber orientation distributions and dispersion. Neuroimage 2018;165:200–221. https://doi.org/10.1016/j.neuroimage.2017.10.046.

[66] Sha Z, Schijven D, Carrion-Castillo A, Joliot M, Mazoyer B, Fisher SE, Crivello F, Francks C. The genetic architecture of structural left-right asymmetry of the human brain. Nat Hum Behav 2021;5(9):1226–1239. https://doi.org/10.1038/s41562-021-01069-w.

[67] Shemesh N, Jespersen SN, Alexander DC, Cohen Y, Drobnjak I, Dyrby TB, Finsterbusch J, Koch MA, Kuder T, Laun F, Lawrenz M, Lundell H, Mitra PP, Nilsson M, Özarslan E, Topgaard D, Westin C-F. Conventions and nomenclature for double diffusion encoding NMR and MRI: Double Diffusion Encoding NMR and MRI. Magn Reson Med 2016;75:82–87. https://doi.org/10.1002/mrm.25901.

[68] Smith S, Nichols T. Threshold-free cluster enhancement: Addressing problems of smoothing, threshold dependence and localisation in cluster inference. NeuroImage 2009;44:83–98. https://doi.org/10.1016/j.neuroimage.2008.03.061.

[69] Smith SM, Jenkinson M, Johansen-Berg H, Rueckert D, Nichols TE, Mackay CE, Watkins KE, Ciccarelli O, Cader MZ, Matthews PM, Behrens TEJ. Tract-based spatial statistics: Voxelwise analysis of

Please cite this article as: I.I. Maximov and L.T. Westlye, Comparison of different neurite density metrics with brain asymmetry evaluation, Z Med Phys, https://doi.org/10.1016/j.zemedi.2023.07.003

multi-subject diffusion data. NeuroImage 2006;31:1487–1505. https://doi.org/10.1016/j.neuroimage.2006.02.024.

[70] Smith SM, Jenkinson M, Woolrich MW, Beckmann CF, Behrens TEJ, Johansen-Berg H, Bannister PR, De Luca M, Drobnjak I, Flitney DE, Niazy RK, Saunders J, Vickers J, Zhang Y, De Stefano N, Brady JM, Matthews PM. Advances in functional and structural MR image analysis and implementation as FSL. NeuroImage 2004;23:S208–S219. https://doi.org/10.1016/j.neuroimage.2004.07.051.

[71] Smith SM, Vidaurre D, Alfaro-Almagro F, Nichols TE, Miller KL. Estimation of brain age delta from brain imaging. NeuroImage 2019;200:528–539. https://doi.org/10.1016/j.neuroimage.2019.06.017.

[72] Szafer A, Zhong J, Gore JC. Theoretical Model for Water Diffusion in Tissues. Magn Reson Med 1995;33:697–712. https://doi.org/10.1002/mrm.1910330516.

[73] Takao H, Hayashi N, Ohtomo K. White matter microstructure asymmetry: Effects of volume asymmetry on fractional anisotropy asymmetry. Neuroscience 2013;231:1–12. https://doi.org/10.1016/j.neuroscience.2012.11.038.

[74] Takao H, Hayashi N, Ohtomo K. White matter asymmetry in healthy individuals: a diffusion tensor imaging study using tract-based spatial statistics. Neuroscience 2011;193:291–299. https://doi.org/10.1016/j.neuroscience.2011.07.041.

[75] Tariq M, Schneider T, Alexander DC, Gandini Wheeler-Kingshott CA, Zhang H. Bingham–NODDI: Mapping anisotropic orientation dispersion of neurites using diffusion MRI. NeuroImage 2016;133:207–223. https://doi.org/10.1016/j.neuroimage.2016.01.046.

[76] Toga AW, Narr KL, Thompson PM, Luders E. Brain asymmetry: evolution. Encyclopedia Neurosci 2009;303–311. https://doi.org/10.1016/B978-008045046-9.00936-0.

[77] Tustison NJ, Avants BB, Cook PA, Zheng Y, Egan A, Yushkevich PA, Gee JC. N4ITK: Improved N3 Bias Correction. IEEE Trans Med Imaging 2010;29:1310–1320. https://doi.org/10.1109/TMI.2010.2046908.

[78] Vellmer S, Edelhoff D, Suter D, Maximov II. Anisotropic diffusion phantoms based on microcapillaries. J Magn Reson 2017;279:1–10. https://doi.org/10.1016/j.jmr.2017.04.002.

[79] Vellmer S, Stirnberg R, Edelhoff D, Suter D, Stöcker T, Maximov II. Comparative analysis of isotropic diffusion weighted imaging sequences. J Magn Reson 2017;275:137–147. https://doi.org/10.1016/j.jmr.2016.12.011.

[80] Veraart J, Novikov DS, Christiaens D, Ades-aron B, Sijbers J, Fieremans E. Denoising of diffusion MRI using random matrix theory. NeuroImage 2016;142:394–406. https://doi.org/10.1016/j.neuroimage.2016.08.016.

[81] Veraart J, Sijbers J, Sunaert S, Leemans A, Jeurissen B. Weighted linear least squares estimation of diffusion MRI parameters: Strengths, limitations, and pitfalls. NeuroImage 2013;81:335–346. https://doi.org/10.1016/j.neuroimage.2013.05.028.

[82] Vinding MS, Brenner D, Tse DHY, Vellmer S, Vosegaard T, Suter D, Stöcker T, Maximov II. Application of the limited-memory quasi-Newton algorithm for multi-dimensional, large flip-angle RF pulses at 7T. Magn Reson Mater Phys Biol Med 2017;30:29–39. https://doi.org/10.1007/s10334-016-0580-1.

[83] Wang Z, Bovik AC, Sheikh HR, Simoncelli EP. Image Quality Assessment: From Error Visibility to Structural Similarity. IEEE Trans Image Process 2004;13:600–612. https://doi.org/10.1109/TIP.2003.819861.

[84] Wei L, Zhong S, Nie S, Gong G. Aberrant development of the asymmetry between hemispheric brain white matter networks in autism spectrum disorder. Eur Neuropsychopharmacol 2018;28:48–62. https://doi.org/10.1016/j.euroneuro.2017.11.018.

[85] Westin C-F, Knutsson H, Pasternak O, Szczepankiewicz F, Özarslan E, van Westen D, Mattisson C, Bogren M, O'Donnell LJ, Kubicki M, Topgaard D, Nilsson M. Q-space trajectory imaging for multidimensional diffusion MRI of the human brain. NeuroImage 2016;135:345–362. https://doi.org/10.1016/j.neuroimage.2016.02.039.

[86] Westlye LT, Walhovd KB, Dale AM, Bjornerud A, Due-Tonnessen P, Engvig A, Grydeland H, Tamnes CK, Ostby Y, Fjell AM. Life-Span Changes of the Human Brain White Matter: Diffusion Tensor Imaging (DTI) and Volumetry. Cereb Cortex 2010;20:2055–2068. https://doi.org/10.1093/cercor/bhp280.

[87] White NS, Leergaard TB, D'Arceuil H, Bjaalie JG, Dale AM. Probing tissue microstructure with restriction spectrum imaging: histological and theoretical validation. Hum Brain Mapp 2013;34:327–346. https://doi.org/10.1002/hbm.21454.

[88] Zhang H, Schneider T, Wheeler-Kingshott CA, Alexander DC. NODDI: Practical in vivo neurite orientation dispersion and density imaging of the human brain. NeuroImage 2012;61:1000–1016. https://doi.org/10.1016/j.neuroimage.2012.03.072.

[89] Zhong S, He Y, Shu H, Gong G. Developmental Changes in Topological Asymmetry Between Hemispheric Brain White Matter Networks from Adolescence to Young Adulthood. Cereb Cortex 2016:bhw109. https://doi.org/10.1093/cercor/bhw109.

[90] Zhou Z, Tong Q, Zhang L, Ding Q, Lu H, Jonkman LE, Yao J, He H, Zhu K, Zhong J. Evaluation of the diffusion MRI white matter tract integrity model using myelin histology and Monte-Carlo simulations. Neuroimage 2020;223:117313. https://doi.org/10.1016/j.neuroimage.2020.117313.

Please cite this article as: I.I. Maximov and L.T. Westlye, Comparison of different neurite density metrics with brain asymmetry evaluation, Z Med Phys, https://doi.org/10.1016/j.zemedi.2023.07.003